Viscous and thermal boundary layers in the detonation driving zone

Hiroaki Watanabe[1], Akiko Matsuo[2], Ashwin Chinnayya[1],
Noboru Itouyama[3], Ken Matsuoka[3], Jiro Kasahara[3]
[1]Institut Prime UPR 3346 CNRS, ISAE-ENSMA, Universite de Poitiers
1 avenue Clément Ader, BP 40109, 86961 Futuroscope-Chasseneuil CEDEX, France
[2]Keio University
3-14-1, Hiyoshi, Kohoku-ku, Yokohama, Kanagawa, 223-8522, Japan
[3]Nagoya University
Furo-cho, Chikusa, Nagoya, Aichi, 464-8603, Japan

1 Introduction

The Chapman-Jouguet (CJ) theory succeeds in predicting the detonation propagation velocity for the ideal case without losses. However, the detonation propagation velocity is known to be affected by boundary conditions due to mass, momentum and energy losses and becomes lower than the CJ velocity [1]. The detonation propagation velocity in tubes and channels is dependent on the inverse of the tube diameter. Several phenomenological models were proposed to explain this trend. Zel'dovich [2] firstly formulated a quasi one-dimensional model, which took into account the wall friction and heat transfer. In addition, Manson and Guénoche [3] proposed that the chemical reactions near the wall were quenched due to the isothermal condition so that only the heat release in the core of the flow contributed to the propagation of the detonation. Furthermore, Fay [4] showed that in the shock frame coordinates, the boundary layer growth induced a negative displacement, influence of which was similar to that of a flow divergence.

These phenomenological models succeeded in reproducing the trend of the propagation velocity with the tube diameter. For example, Shi et al. [5] compared their experimental results with the models of Zel'dovich and Fay, and the velocity deficits in the loss governed regime were well captured by Zel'dovich model. However, the characteristics of the boundary layer such as the skin coefficient and the displacement thickness are required in the models of Zel'dovich and Fay, respectively. Moreover, the determination of the skin friction and the heat flux are of major concerns for detonation combustors. Chinnayya et al. [6] and Sow et al. [7] numerically studied the characteristics of the viscous boundary layer behind the detonation propagating in narrow channels. The Reynolds number and the power exponent of the displacement thickness suggested that the viscous boundary layer could be considered to be laminar. They also found that the boundary layer got thinner and the skin coefficient was higher than that of the Blasius law. Xiao et al. [8] indicated that the boundary layer behind H_2/O_2/Ar detonations was laminar from the value of the Reynolds number, which was estimated using the ZND model with lateral strain rate. In addition, the boundary layer induced losses was evaluated from the $D_n - \kappa$ curve in two different exponential diverging channel experiments. Furthermore, Damazo et al. [9] experimentally investigated the heat flux behind stoichiometric hydrogen detonations and the heat transfer rate was consistent with the prediction for laminar boundary layer.

Correspondence to: watanabe0204@keio.jp, hiroaki.watanabe@ensma.fr

Nevertheless, the understanding of the boundary layer behind the detonation front is still limited up to now. Moreover, there were no numerical attempt to obtain the mean characteristics of the viscous and thermal boundary layer behind the leading front in a two-dimensional (2D) straight channel. To address this problem, 2D numerical simulations with detailed chemistry were performed in order to characterize the viscous and thermal boundary layers in the mean detonation driving zone (DDZ), which is the relevant region for its propagation.

2 Numerical setup and problem statement

The governing equations for the gaseous phase are the 2D reactive compressible Navier-Stokes equations, with the ideal equation of state. The chemical reaction mechanism proposed by Hong et al. [10], which considers 9 species (H_2, O_2, H, O, OH, H_2O, HO_2, H_2O_2 and Ar) and 20 elementary reaction, is used. The other numerical models and methods were the same as our previous study [11].

The fully developed two-dimensional gaseous detonation propagated in a two-dimensional straight channel. Two types of reactive mixtures have been investigated: 70% diluted stoichiometric hydrogen oxygen mixture $2\,H_2 - O_2 - 7\,Ar$ and stoichiometric hydrogen oxygen mixture $2\,H_2 - O_2$ at ambient conditions (0.1 MPa and 300 K). Thus the effect of the instabilities on the mean characteristics of the boundary layer can be assessed. The channel widths for $2\,H_2 - O_2 - 7\,Ar$ and $2\,H_2 - O_2$ mixtures are 2.6 mm and 2.0 mm, respectively. In addition to the two types of reactive mixtures, two types of the non slip wall condition, i.e. adiabatic and isothermal wall at 300 K were simulated to study the viscous and thermal boundary layers. The outflow boundary was applied to the left end. The grid was uniform and was equal at 2.0 μm and 1.6 μm from the region from the shock front up to 20.6 mm and 11.5 mm behind the front for the $2H_2$-O_2-7Ar mixture and $2H_2$-O_2 mixture, respectively. Then, the grid was stretched. The grid resolution was about 38 and 30 points per the CJ induction length (x_{ind}) for $2H_2$-O_2-7Ar mixture and $2H_2$-O_2 mixture, respectively. This resolution has been shown to be largely sufficient to capture the mean structure [12]. The recycling block technique [7] was applied to enable the detonation to propagate a distance long enough to obtain statistical values. The length of the propagation for the average procedure was about 1000 x_{ind} for $2\,H_2 - O_2 - 7\,Ar$ mixture and 1200 x_{ind} for $2\,H_2 - O_2$ mixture. The average cell width in the simulations was estimated as 1.3 mm and 0.7 mm for $2\,H_2 - O_2 - 7\,Ar$ mixture and $2\,H_2 - O_2$ mixture. The average propagation velocity agreed with the CJ velocity in the present conditions. The Favre average 2D flow field in the instantaneous shock frame [7] was obtained to evaluate the mean characteristics of the viscous and thermal boundary layers.

3 Results and discussions

Figure 1 depicts the Favre average 2D flow fields for the x-velocity in the shock frame for two reactive mixtures and the two wall conditions. The development of the negative displacement thickness could be clearly seen in Fig. 1, as in the Fay model and the previous numerical studies [6, 7]. After the passage of the leading shock front, the flow in the core region was accelerated by the exothermic chemical reaction and the momentum diffusion from the non-slip wall.

The note to point out was that the viscous boundary layer for the case with the isothermal wall at 300 K was thicker than that with the adiabatic wall, even though the general picture was the same. The kinematic viscosity near the adiabatic wall became larger than that with the isothermal wall and their ratio was about 60 and 160 times for $2\,H_2 - O_2 - 7\,Ar$ and $2\,H_2 - O_2$ mixtures, respectively. This resulted in the thicker viscous boundary layer in the case with isothermal wall for the same reactive mixture, especially for the non-diluted mixture.

The Favre average 2D flow fields for the temperature and OH mass fraction for the two reactive mixtures with isothermal wall condition are shown in Fig. 2. The thermal boundary layer developed behind the leading shock front of detonation. The thickness of the thermal boundary layer was slightly

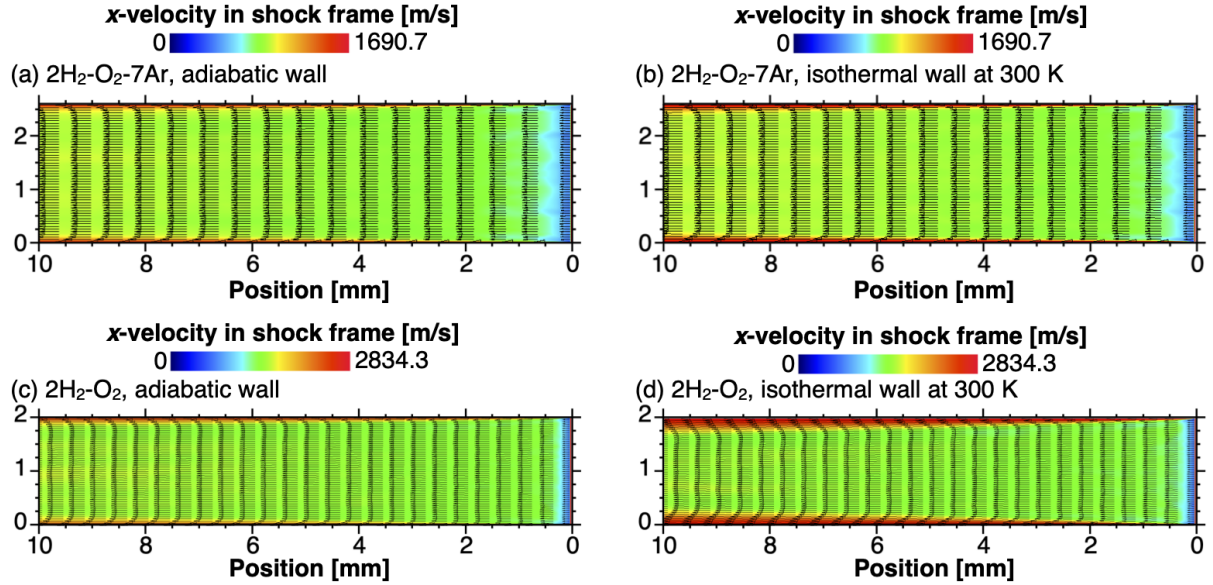

Figure 1: Favre averaged 2D flow fields for x-velocity in shock frame. (a) $2\,H_2-O_2-7\,Ar$ mixture with adiabatic wall, (b) $2\,H_2-O_2-7\,Ar$ mixture with isothermal wall at 300 K, (c) $2\,H_2-O_2$ mixture with adiabatic wall, (d) $2\,H_2-O_2$ mixture with isothermal wall at 300 K. Black arrows represent the velocity vectors in the shock frame.

larger than that of the viscous boundary layer as Prandtl number was about 0.72 and 0.85 inside the thermal boundary layer for the diluted and non-diluted mixtures, respectively. However, the distributions of the chemical species inside the thermal boundary layer were different from those outside and the chemical reactivity inside the thermal boundary layer was also not active, as envisioned by Manson and Guénoche [3]. Moreover, the mass fraction of H_2O inside the thermal boundary layer for the diluted and non diluted mixture at 200 x_{ind} behind the front was 0.11 and 0.95, respectively. Therefore, the effect of the condensation could be expected to play a role. Owens et al. [13] also pointed out that the modeling of wall water condensation was needed to have a better estimation of wall losses, for performance estimations.

The skin coefficient and Stanton number as a function of local Reynolds number are illustrated in Fig. 3. The skin coefficient c_{f} , Stanton number St and Reynolds number Re were defined by the following equations, referring to the previous study on the shock induced laminar boundary layer of Mirels [14].

$$c_{\mathrm{f}} = \frac{\tau_{\mathrm{w}}}{\frac{1}{2}\rho_{\mathrm{w}} u_{\mathrm{lab,c}}^2}, \tau_{\mathrm{w}} = \left(\mu \frac{\partial u}{\partial y}\right)_{\mathrm{w}} \tag{1}$$

$$\mathrm{St} = \frac{\dot{q}_{\mathrm{w}}}{\rho_{\mathrm{w}} u_{\mathrm{lab,c}} (h_{\mathrm{c}} - h_{\mathrm{w}})}, \dot{q}_{\mathrm{w}} = \left(\lambda \frac{\partial T}{\partial y}\right)_{\mathrm{w}} \tag{2}$$

$$\mathrm{Re} = \frac{u_{\mathrm{shock,c}} x_{\mathrm{s}}}{\nu_{\mathrm{w}}} \tag{3}$$

Here, τ_{w}, ρ_{w}, $u_{\mathrm{lab,c}}$, μ, $\dot{q}_{\mathrm{w}}$, h_{c}, h_{w}, λ, $u_{\mathrm{shock,c}}$, x_{s}, and ν_{w} are the wall shear stress, density on the wall, x-velocity in laboratory frame at the center line, viscosity, wall heat flux, enthalpy at the center line, enthalpy on the wall, thermal conductivity, x-velocity in shock frame at the center line, the distance from leading shock front, and the kinematic viscosity on the wall, respectively.

The skin coefficients followed the same similar trend for the same wall condition regardless of the mixture instabilities. However, the isothermal case was always lower than the adiabatic case.

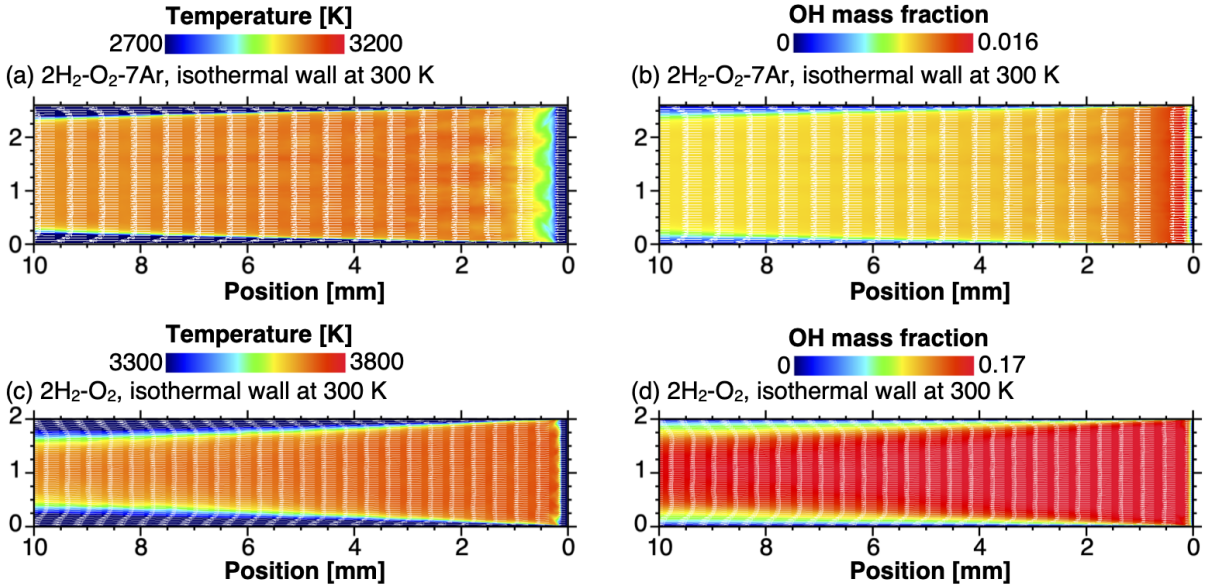

Figure 2: Favre averaged 2D flow fields for temperature and OH mass fraction, with isothermal wall at 300 K. Top: $2\,H_2-O_2-7\,Ar$ mixture, (a) temperature, (b) OH mass fraction. Bottom: $2\,H_2-O_2$ mixture, (c) temperature, (d) OH mass fraction. White arrows are the velocity vector in the shock frame.

Table 1: Coefficients of the skin coefficient $c_f \propto Re^{-\alpha}$ for the adiabatic case.

Adiabatic case	Region 1	Region 2
$2H_2$-O_2-7Ar	0.09	0.63
$2H_2$-O_2	-0.13	0.60

Table 2: Coefficients of the skin coefficient $c_f \propto Re^{-\alpha}$ for the isothermal case, $T_w = 300\,K$.

Isothermal case	Region 1	Region 2
$2H_2$-O_2-7Ar	0.16	0.93
$2H_2$-O_2	0.59	-

The skin coefficient could be approximated piecewise as $c_f \propto Re^{-\alpha}$. From the graphs, two regions could be distinguished with different values of the α coefficient, which are given in Tables 1 and 2.

The α coefficient in the two regions was different from the suggestion of Mirels for turbulent flow of 0.2. It was closer to the laminar behavior of 0.5 for the cases with adiabatic wall for region 2. It differs also with Sow's [7] estimate of ~ 1, determined for very weakly unstable cases. Previous experimental results [8, 9] have highlighted that the flow downstream of the front was most probably laminar.

The Reynolds number where the slope for the skin coefficient was most different from the theory without pressure gradient in the region 1 correspond to the region where the thermicity and the pressure gradient were the highest. In addition, separation in the viscous boundary layer was observed and was located at around 6.5 to 9.0 x_{ind} behind the front for $2\,H_2-O_2$ mixture with the isothermal wall condition. The viscosity was lower near the isothermal wall at 300 K and thus the separation was perhaps more prone to occur than in the case with adiabatic wall. Moreover, the boundary layer could be separated due to the strong adverse pressure gradient induced by the interaction of the transverse

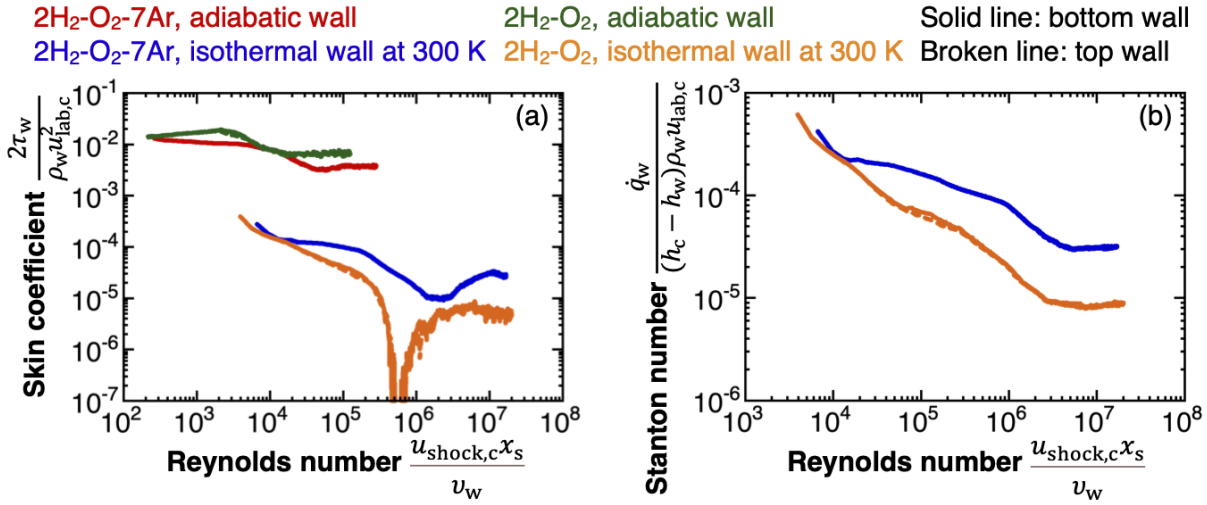

Figure 3: Favre averaged 1D profiles for the (a) skin coefficient, (b) Stanton number as a function of Reynolds number.

Table 3: Coefficients of the Stanton number $\mathrm{St} \propto \mathrm{Re}^{-\alpha}$ for the isothermal case, $T_\mathrm{w} = 300\,\mathrm{K}$.

Isothermal case	Region 1	Region 2	Region 3
$2H_2$-O_2-7Ar	0.18	0.30	0.64
$2H_2$-O_2	0.73	0.35	0.73

waves with unburnt pockets near the isothermal wall.

Given that Cohen et al. [15] showed that the pressure gradient affected the shear stress and the Reynolds analogy for laminar compressible flow, the pressure gradient can be considered to be the factor for the change in the slope for the skin coefficient. Other possible reasons could be the repeated impingement of the transverse waves on the boundary layer and the separation of the boundary layer. These might be the reasons why Kitano et al. [16] increased the skin coefficient in Zel'dovich 1D model to match the experimental results.

The curve for Stanton number showed a similar trend for the two mixtures. The first change of slope was also observed for the region with high pressure gradient and thermicity. The Stanton number could also be approximated piecewise as $\mathrm{St} \propto \mathrm{Re}^{-\alpha}$. From the graphs, three regions could be distinguished before the plateau value, with different values of the α coefficient, which are given in Table 3.

Far behind the front, the skin coefficient in the adiabatic wall cases was similar to the values of 5×10^{-3} estimated by Edward et al. [17] from the pressure, velocity and heat flux measurements and 6.2×10^{-3} calibrated against the experimental measurement of heat flux by Radulescu et al. [18]. This might be the reason why the constant value of 6.2×10^{-3} worked well for the prediction of the performance losses [13, 18]. Note that the comparable values for the skin coefficient could be obtained in the isothermal case if the density in the center line was used for the definition of skin coefficient.

The maximum wall heat flux was estimated as $20\,\mathrm{MW/m^2}$ and $131\,\mathrm{MW/m^2}$ for the diluted and non-diluted mixture, respectively. The experimental value for the wall heat flux was reported to be $8\,\mathrm{MW/m^2}$ at $100\,\mu\mathrm{s}$ for $2\,H_2 - O_2$ mixture at an initial pressure of 101 kPa [20] and $10\,\mathrm{MW/m^2}$ at $100\,\mu\mathrm{s}$ for $2\,H_2 - O_2$ mixture at 50 kPa [19]. In the present simulation, the heat flux for $2\,H_2 - O_2$ mixture at 100 kPa became $1\,\mathrm{MW/m^2}$ at the end of the domain around $7\,\mu\mathrm{s}$. The discrepancy between these experiments and the simulations might be due to the transition from laminar to turbulent boundary layer

in the experiments, downstream of the mean DDZ. This indicated that the flow beyond the hydrodynamic thickness was important for the estimation for the heat flux. Indeed, the hydrodynamic thickness estimated from the 1D Favre average profile is 148.0 x_{ind} and the Reynolds number at the hydrodynamic thickness is about 1.44×10^7. In fact, from Chinnayya et al. [6], the 2D detonation driving zone is known to be non-planar, with the same topology as in condensed phase case. The hydrodynamic thickness is taken here to be the distance between the mean sonic line and the leading shock. The hydrodynamic distance encompasses the DDZ.

4 Conclusions

Viscous and thermal boundary layers developed behind the leading shock front. The flow was then accelerated by the exothermic chemical reactions and the momentum diffusion from the wall. In the isothermal case, the thermal boundary layer also caused the change in the reactivity, as highlighted by Manson and Guénoche. The first change of the slope of the curve for the skin coefficient and Stanton number was related of the thermicity peak, which induced the highest pressure gradient. The isothermal and adiabatic cases were very different. The Stanton number for both mixtures showed the similar trend regardless of the cell structure regularity. Different scaling laws have been obtained in different regions in the DDZ, which can be used in models for detonations with wall losses.

Acknowledgements

This research was subsided by JSPS KAKENHI Grant number JP20K22391(Grant-in-Aid for Research Activity Start-up), JP21K14094(Grant-in-Aid for Early-Career Scientists), JP19J12758(Grant-in-Aid for Specially Promoted Research), the Paloma Environmental Technology Development Foundation, and the CPER FEDER Project of Région Nouvelle Aquitaine and pertains to the French government program "Investissements d'Avenir" (EUR INTREE, reference ANR-18-EURE-0010). HW is supported by JSPS Overseas Research Fellowships.

References

[1] Lee J.H.S. (2008). The detonation phenomenon. Cambridge University Press.
[2] Zel'dovich Y.B. (1950). On the theory of the propagation of detonation in gaseous systems. NACA Tech. Momorandum 1261.
[3] Manson N., Guénoche H. (1957). Effect of the charge diameter on the velocity of detonation waves in gas mixtures. Proc. Combust. Inst. 6: 631.
[4] Fay J.A. (1959). Two-dimensional gaseous detonations: velocity deficit. Phys. Fluids 2: 283.
[5] Shi X., Crane J., Wang H. (2021). Detonation and its limit in small tubes with ozone sensitization. Proc. Combust. Inst. 38: 3547.
[6] Chinnayya A., Hadjadj A., Ngomo D. (2013). Computational study of detonation wave propagation in narrow channels. Phys. Fluids 25: 036101.
[7] Sow A., Chinnayya A., Hadjadj A. (2019). On the viscous boundary layer of weakly unstable detonations in narrow channels. Comput. Fluids 179: 449.
[8] Xiao Q., Radulescu M.I. (2020). Dynamics of hydrogen-oxygen-argon cellular detonations with a constant mean lateral strain rate. Combust. Flame 215: 437.
[9] Damazo J.S., Odell J., Shepherd J.E. (2012). Boundary layer profile behind gaseous detonation as it affects reflected shock wave bifurcation. 42nd AIAA Fluid Dynamics Conference and Exhibit, 2975.
[10] Hong Z., Davidson D.F., Hanson R.K. (2012). An improved H2/O2 mechanism based on recent shock tube/laser absorption measurements. Combust. Flame 158: 633.
[11] Watanabe H., Matsuo A., Chinnayya A., Matsuoka K., Kawasaki A., Kasahara J. (2020). Numerical analysis of the mean structure of gaseous detonation with dilute water spray. J. Fluid Mech. 887: A4.
[12] Reynaud M., Taileb S., Chinnayya A. (2020) Computation of the mean hydrodynamic structure of gaseous detonation with losses. Shock Waves 30: 645.
[13] Owens Z.C., Hanson R.K. (2010) The influence of wall heat transfer, friction, and condensation on detonation tube performance. Combust. Sci. Tech. 182: 1104.
[14] Mirels H. (1956) Laminar boundary layer behind shock advancing into stationary fluid. NACA Technical note 3401.
[15] Cohen C.B., Reshotko E. (1956) Similarity solutions for the compressible laminar boundary layer with heat transfer and arbitary pressure gradient. NACA Technical Note 3325.
[16] Kitano S., Fukao M., Susa A., Tsuboi N., Hayashi AK., Koshi M. (2009) Spinning detonation and velocity deficit in small diameter tubes. Proc. Combust. Inst. 32: 2355.
[17] Edwards D. H., Brown D. R., Hooper G., Jones A. T. (1969) The influence of wall heat transfer on the expansion following a C-J detonation wave. J. Phys. D. Appl. Phys.. 3: 365.
[18] Radulescu M. I., Hanson R. K. (2005) Effect of heat loss on pulse-detonation-engine flow field and performance. J. Propul. Power 21: 274.
[19] Damazo J.S. (2013). Planar reflection of gaseous detonations. PhD thesis, California Institute of Technology.
[20] Laderman A.J., Hecht G.J., Oppenheim A.K. (1962). Thin film thermometry in detonation research. In Herzfeld CM editor, Temperature - its measurement and control in science and industry, Vol. 3.